Missile Grid Fins Analysis using Computational Fluid Dynamics: A Systematic Review

Nayhel SHARMA*,[1], Rakesh KUMAR[1]

*Corresponding author
*,[1]Aerospace Engineering Department, Punjab Engineering College
(Deemed to be University),
Sector 12, Chandigarh, 160012-India,
nayhel.sharma@gmail.com*, rakeshkumar@pec.ac.in

DOI: 10.13111/2066-8201.2019.11.1.12

Received: 23 October 2018/ Accepted: 14 December 2018/ Published: March 2019
Copyright © 2019. Published by INCAS. This is an "open access" article under the CC BY-NC-ND license (http://creativecommons.org/licenses/by-nc-nd/4.0/)

Abstract: *Grid Fins are unconventional control surfaces, consisting of cells in an outer frame. Uniqueness of Grid Fins is that they are aligned parallel to the direction of air flow. The orientation of these fins results in aerodynamic demerits such as choking of flow inside the cells and thereby resulting in increased drag forces. Both experimental and Computational Fluid Dynamics (CFD) studies have been employed in negating these effects. This paper reviews the work done by various authors to overcome the anomalies using CFD approach. This paper also discusses the measures to overcome these anomalies. The paper presents an insight and step by step guidelines for CFD simulations right from the pre-processing to the post-processing.*

Key Words: *Computational Fluid Dynamics, Aerodynamics, Grid Fins*

1. INTRODUCERE

Grid Fins are an unconventional control surfaces, consisting of a frame with intersecting thin walls. The interesting thing about these fins is, that they are aligned facing in the direction of airflow. They have a small chord length as compared to the conventional planar fins, thus experience lesser hinge moments. They display higher lift characteristics at higher angles of attack. Because of small chords and smaller hinge moments, they utilize smaller actuators to move them even at high speed flows. These fins are also used as deaccelerating control and stabilizing surfaces in spacecrafts. These fins can be manufactured having both radius-to-curvature frame of a flat frame. Thus, these fins envelop the missile body when in stored, transport or unlaunched condition. These grid fins are utilized mainly in the medium air-to-air cruise missiles, to name some AA-12 based Russian R-77 and US AMRAAM [1]. Few of more practical applications in which grid fin control can be seen are listed in *Table I*. The small chords also make them efficient at high angles of attack as compared to the planar fins. Also, the inner web structure provides with excellent strength to weight ratios, making them more apt for high speed travelling. At supersonic speeds they have much reduced drag values as compared to the conventional planar fins, making grid fins a better control surface even after experiencing forces equal to 12Gs and for long duration flight paths. Many Grid fin configurations have been tested in the past using both experimental as well as CFD methods for reduction of drag in the transonic regime. CFD is a reliable tool which is recommended for studying various flow fields of the missiles having grid fins. The CFD pressure measurements in the grid fin region as well as on the missile surface can be easily verified. In addition to these measurements, CFD can be used as a tool for studying the tedious part of flow visualization in-between the cells thus helping to avoid the choking of cells in the transonic regime.[2] Montgomery et.al discuss the effects of the sub scaled models in the experimental as well as CFD studies, also determining the critical Mach number for different Mach numbers.[3] 30% of the longitudinal stability is provided by the vertical fins alone [4]. Experimental investigations carried out by Miller et.al to determine the effects of outer frame cross-section, shape and web thickness, show significant effects of the fin geometry on fin aerodynamics [5]. The results of wind tunnel tests comparing the grid fins to the conventional planar fins, performed by Fournier [6] show the unfavorable aspects of the grid fins. Theerthamalai & Nagarathinam state a method based on shock-expansion theory for estimation of aerodynamic characteristics of the grid fins [7]. For the subsonic flows, aerodynamic characterization has been done using vortex lattice network methodology, which held good for angle of attacks up to 25° [8]. Reynier et.al state a flow prediction theory for missiles having grid fins based on actuator disc concept, coupled with unstructured Navier-Stokes equations [9,10]. A theoretical approach using vortex lattice methods imbibing the up-wash terms and load predictions has been proposed by Burkhalter et.al [11]. This theory predicts the aerodynamic coefficients and gives results in parallel with the experimental data for the missiles having grid fins, for angles of attack up to 20°. The reduction of drag by employing sweptback grid fins (with sharp leading edge) and their comparison with the baseline grid fin, both experimentally and numerically (CFD) has been done by Marco Debiasi et.al. [12–14]. Comparison between the blunt and the sharp leading edges of swept-back grid fins and baseline fins has been performed by Yan Zeng [15]. The CFD study done by Chen et. al [16] indicates degradation in grid fin performance using thick fin panels. The free flight tests conducted by Abate et.al explain aerodynamics related to the scaling of grid fin models in the transonic regime. The thinning of fin blades and the use of lesser number of webs show a reduction in the drag values of the grid fins. Critical Mach numbers have also been reported in the free flight testing of Grid fin baseline and sub scaled models [17]. A locally swept back lattice fin was proposed consisting of “Peak” type and “Valley” type locally swept Back fins. A considerable drag reduction is seen in those locally swept-back fins from the experimental as well as CFD results, also an increase in lift values is reported for these fin configurations [18]. The experimental and CFD study on the effect of grid fins on missiles having canard wings have been performed both in the subsonic and transonic flows [19]. A study by Misra shows the aerodynamics associated with the cascade fins and their advantages at high angles of attack [2]. It is an interesting computational study involving 2D and 3D grid fins in which a two-dimensional five plate approach towards grid fins can be seen [20]. The overall data available for the grid fins consists of mainly static aerodynamic coefficients and stability derivatives; however new researches have come up with the dynamic aerodynamic coefficients as well. A liner subsonic analysis, transonic analysis compared with the bucket effect and supersonic linear and non-linear analysis for the development of an aerodynamic prediction code of grid fins is discussed in reference [21]. This prediction code has been done for a missile dropped from an aero plane flying at a velocity of 150.2 m/s at an altitude of 7001.40 m.

Table I: projectiles utilizing grid fins [2,22]

Grid fin Controlled Projectiles	
Name/ Code	**Type**
R-77 (AA-12)	Russian medium range air-to-air missile
AMRAAM	US missile

SS-20 “saber” SS-21 “scarab” SS-23 “spider”	Ballistic Missiles
MOAB	Massive ordnance blast bomb
N1 lunar rocket Soyuz TM-22	As brakes in Russian spacecrafts
Quick MEDS	Material express Delivery systems for unmanned Aircraft systems

This paper discusses the basic aerodynamics of the grid fins, its drawbacks and the measures taken up in the past by the researchers to overcome them. Focusing on the computational Fluid Dynamics part this paper discusses the pre- analysis methods, describing behind the scene mathematical approaches. Along with that, the wall modelling strategies, which are of utmost importance in understanding the near wall behavior of the fluid flow, have been discussed. Various geometries with their uniqueness have been mentioned as careful and accurate modelling of the missiles result in better aerodynamic calculations and for comparison and validation purpose. The next part discusses the handling of domain and the mesh for the grid fin missiles, how the symmetry of the missile and the fin can be utilized as an advantage by taking only the half, one fourth or in some cases even one-eighth of the body for analysis. It also gives an insight to the cumbersome process of creating a uniform mesh in between the grid fin cells. The physical setup and the boundary conditions are by and large the same, the computational step is briefly defined covering all the used turbulent models, their boundary conditions and the methods used for computing of these models. In the end the validation and verification of the CFD process in which the convergence parameters along with the range of the previously performed CFD analysis have been approached. This paper will systematically guide the researcher in each step of the CFD analysis on grid fins.

2. AERODYNAMIC CHARACTERISTICS OF THE GRID FIN MODEL

The missiles using grid fins show greater aerodynamic control and long-range stability as compared to the conventional planar fins. The assumed flow structure inside the grid fins is compressible in the subsonic regime, chocked in the transonic and transition from shock reflections to un-reflected shocks in increasing supersonic regime [22]. In general, the design of the fins, the fin shape, fin thickness, leading edge sharpness etc., play a major role in the aerodynamics of the grid fins. The choking may occur in a few cells; however, their implications are tremendous. Having excessive drag as compared to the conventional fins, these fins often find their positive use as a braking surface or control surface in bombs or low range missiles. Using swept-back grid fins (frame) with sharp leading edges indicate a reduction of drag up to 30% at zero angle of attack. The freestream velocity shows an increase till Mach 1.1 after which it may show choking of the cells. At supersonic flows there is less drag with the choking of cells almost negligible [13]. The normal shock is swallowed and the shock passes through the cells without interfering with the grid fin structure in the supersonic regime. Adding 20°sharp angle at the leading edge further reduces the drag of the swept-back grid fins in the trans-sonic & the supersonic regimes [14]. The drag reduction benefit can be utilized at non- zero angle of attack as well [15]. Experimentally, it has been shown that sweeping of complete fins in forward direction increases the drag. In case of sweeping forward 10% more drag is observed [22]. The grid fin cross-section frame shape and web thickness show a minimal effect on normal force characteristics [6]. The CFD studies have revealed that in the transonic regime an expansion and compression flow waves are formed which incubate a compression shock ahead of the grid fin structure. This phenomenon has been attributed to the choking of grid fin cells as the Mach number increases (beyond the transonic regime), local oblique shocks are formed with the absence of choking of flow inside the cells [16]. The flow characteristics of the Grid Fins have often been given an analogy of flow through a nozzle. The sweptback fins act as a source of increasing of effective nozzle length thus avoiding the choking of cells and ultimately reduction of drag [23]. Mach 0.90 has been a focal point of research in the trans-sonic regime showing maximum drag forces. Beyond Mach 2.8 in the supersonic regime, no choking of cells has been reported. A reduction in static stability and reduced normal force has been reported in the wind tunnel experiments ranging from 0.5M to 3.0M [24]. The use of grid fins doesn't improve much the flow characteristics of canard wings in the transonic regime as compared to the supersonic regime [20]. The grid fins fail to provide much advantage to the canard fins in the subsonic flow, especially at angle of attack greater than α = 4°, they show signs of adverse rolling moments and induce side forces [25]. The Vortex lattice formulation are inviscid solutions, which have been employed by many in the past; they are valid for linear angle of attack range only i.e. up to α = 20° [2]. The use of "optimized Busemann" fin profile in grid fins has been tested both statically and dynamically, [26] show better results for reduction of drag in the supersonic regime. The canard wings produce trailing vortices which result in adverse induced side forces, the grid fins at the tail end can help in negating this effect and thereby improve the roll effectiveness of canards, especially at low supersonic speeds [27]. It should be noted that in some cases the force coefficient may converge ahead of the global convergence criterion. The sharp leading-edge fins show a trend towards reduction of the fin axial force. The fins having blunt edges, show uneven pressure differences aft of the fin structure, whereas the fins having swept back sharp edges show uniform expansion and contracting flow characteristics. At around Mach 1.70M, after crossing the trans-sonic regime, the fins having blunt edges show a formation of shock much ahead of the leading fin edge, which is not there in the case of swept back fins. This also indicates a smoother behavior of sweptback sharp leading-edge fins in the supersonic regime. *Figure 1* shows the flow approaching the blunt and sweptback sharp leading-edge fins, respectively. Mach number contours passing through the grid fins have been compared at different Mach numbers [13]. The "X" pattern of the flow behind the fins indicates its expansion and the contraction; this causes difference in the pressure values aft of the fin body and thus incubates shock structures [14]. The aerodynamic drag coefficients are calculated by adding the viscous and the pressure forces in the post processing [16]. The reference area for the same is taken as one eighth of the cross-sectional area of the missile base, the reference length is taken as the missile diameter.

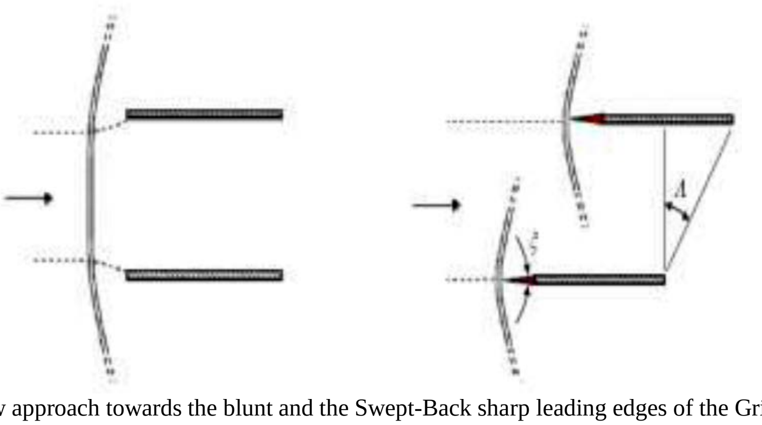

Figure 1: Flow approach towards the blunt and the Swept-Back sharp leading edges of the Grid Fins [13]

3. PRE-ANALYSIS/ MATHEMATICAL MODELS CFD APPROACH

The maximum simulations have been done using the turbulence methods. Though inviscid and laminar analysis on grid fins have also been done in the past, turbulence modelling remains the most apt one. Turbulence modelling is an important component in simulating high speed flows or high Reynolds number flows. There is no single turbulence model which can have universal acceptance for solving the CFD problems. Turbulence is basically the fluctuation of low frequency, high frequency or even a combination of both. These fluctuations consist of mix transport quantities such as momentum and energy. Choosing a turbulence model depends upon the model geometries and computational capabilities of the processors. The time averaged Reynolds Averaged Navier-Stokes equation (RANS) models can be one equation Spalart-Allmaras model, the two equations K $-\ \varepsilon$ family and the $\kappa - \omega$ family models, the Reynolds Stress Models and the Transition Models (i.e. the $\kappa - \kappa I - \omega$, transition shear stress transport (SST) models). Three dimensional Navier-Stokes equations with a turbulence model are preferred for the turbulent flow field. [13, 14] These are expressed as follows:

$$\frac{\partial \rho}{\partial t}+\frac{\partial}{\partial x_j}\left(\rho u_j\right)=0 \tag{1}$$

$$\frac{\partial}{\partial t}\left(\rho u_j\right)+\frac{\partial}{\partial x_j}\left(\rho u_j u_i\right)=-\frac{\partial p}{\partial t}+\frac{\partial \hat{\tau}_{ji}}{\partial x_j} \tag{2}$$

$$\frac{\partial}{\partial t}\left(\rho E\right)+\frac{\partial}{\partial x_j}\left(\rho u_j H\right)=\frac{\partial}{\partial x_j}\left[u_i\hat{\tau}_{ji}+\left(\mu+\sigma*\mu_T\right)\frac{\partial k}{\partial x_j}-q_j\right] \tag{3}$$

Where $\boldsymbol{t}$ is the time, $\boldsymbol{x_i}$ the position vector, $\boldsymbol{\rho}$ the density, $\boldsymbol{u_i}$ the velocity vector, $\boldsymbol{p}$ the pressure, $\boldsymbol{\mu}$ the dynamic viscosity. The total energy and enthalpy are $\boldsymbol{E} = e + k + u_i u_j/2$ and $\boldsymbol{H} = e + p/\rho + k + u_i u_j/2$, respectively, with $\boldsymbol{e} = p/[(\gamma - 1)\rho]$. The $\boldsymbol{\gamma}$ is the ratio of specific heats at constant pressure and constant volume. Other quantities are defined in the equations below:

$$\mu_T=\rho v_t \tag{4}$$

$$S_{ij}=\frac{1}{2}\left(\frac{\partial u_i}{\partial x_j}+\frac{\partial u_j}{\partial x_i}\right) \tag{5}$$

$$\tau_{ij}=2\mu_T\left(S_{ij}-\frac{1}{3}\frac{\partial \mu_k}{\partial x_k}\delta_{ij}\right)-\frac{2}{3}\rho k\delta_{ij} \tag{6}$$

$$\hat{\tau}_{ij}=2\mu\left(S_{ij}-\frac{1}{3}\frac{\partial u_k}{\partial x_k}\delta_{ij}\right)+\tau_{ij} \tag{7}$$

$$q_j=-\left(\frac{\mu}{p_{T_L}}+\frac{\mu_T}{p_{T_T}}\right)\frac{\partial h}{\partial x_j} \tag{8}$$

$$k=\frac{1}{2}\mu'_j\mu'_i \tag{9}$$

where $\boldsymbol{\delta}_{ij}$ indicates the Kronecker delta, and $\boldsymbol{\mu}'_i$, is the fluctuation of the velocity component $\boldsymbol{u}_i$. The 3D, time dependent RANS equations are solved using the finite volume method:

$$\frac{\partial}{\partial t}\int_v \boldsymbol{W} dV + \oint [\boldsymbol{F} - \boldsymbol{G}] \cdot d\boldsymbol{A} = \int_v \boldsymbol{H} dV \tag{10}$$

where, **W** is the vector of conservative variables, and ***F*** and ***G*** are the inviscid and viscous flux vectors, respectively, defined as

$$\boldsymbol{W} = \begin{Bmatrix} \rho \\ \rho u \\ \rho v \\ \rho w \\ \rho E \end{Bmatrix}, \quad \boldsymbol{F} = \begin{Bmatrix} \rho v \\ \rho v u + p i \\ \rho v v + p j \\ \rho v w + p k \\ \rho v E + p v \end{Bmatrix}, \quad \boldsymbol{G} = \begin{Bmatrix} 0 \\ \tau_{xi} \\ \tau_{yi} \\ \tau_{zi} \\ \tau_{ij} v_j + q \end{Bmatrix} \tag{11}$$

where, ***H*** is the vector of source terms, ***V*** is the cell volume, and ***A*** is the surface area of the cell face [28]. In considering the grid fin cells as a nozzle, the area-Mach number relation in quasi-one-dimensional nozzle and critical transonic Mach number, which cause sonic conditions at the throat with formation of a normal shock the following equation is used [3].

$$\left(\frac{A}{A*}\right)^2 = \frac{1}{M_\infty^2 \left[\frac{2}{\gamma+1}\left(1 + \frac{\gamma+1}{2} M_\infty^2\right)\right]} \tag{12}$$

Also, in terms of vane spacing ***V*** and fin thickness ***t***, the area ratio is defined as:

$$\left(\frac{A}{A*}\right)^2 = \frac{(v+t)^2}{v^2} \tag{13}$$

where, ***A*** is the cell reference area for area-Mach number relation, $\boldsymbol{A*}$ throat area for sonic flow from quasi one-dimensional flow theory, $\boldsymbol{M}_\infty$ freestream Mach number, $\boldsymbol{\gamma}$ is the ratio of specific heats. The near-wall treatment for the boundary layer profile prediction is done by making the velocity and the wall distance dimensionless. The velocity is made dimensionless, by dividing the velocity with shear velocity near the wall of the turbulent flow $\boldsymbol{U}/\boldsymbol{U}_{\boldsymbol{\tau}}$ where $\boldsymbol{U}_{\boldsymbol{\tau}} = \sqrt{\frac{\boldsymbol{T}_{wall}}{\boldsymbol{\rho}}}$. The wall distance is made dimensionless $\boldsymbol{y}^+ = \boldsymbol{y}\boldsymbol{U}_{\boldsymbol{\tau}}/\boldsymbol{\upsilon}$ where ***y*** is the distance from the wall and $\boldsymbol{\upsilon}$ is the dynamic viscosity of the fluid. A predictable boundary profile is obtained using these dimensionless quantities. The wall modelling strategies for the near wall treatment use the wall function approach in which a typical y^+ value is such that $30 < y^+ < 300$ and where resolving of viscous sub layer is required $y^+ \approx 1$ is set with the mesh growth rate not greater than ≈1.2, which is related directly to the inflation layers. Also,

$$\mathrm{Re}_L = \frac{\rho . U_\infty . L}{\mu} \tag{14}$$

$$\tau_{wall} = \frac{c_f \rho U_\infty^2}{2} \tag{15}$$

$$c_f = \frac{0.026}{\mathrm{Re}_x^{1/7}} \tag{16}$$

4. GEOMETRY

Various geometries have been used in the experimental and the CFD simulations. A 3D length tangent ogive nose and 13D long cylindrical after body and another missile body with 3D length tangent ogive nose with 10D long missile afterbody are the most commonly used missile dimensions. All the dimensions are considered with respect to missile diameter D. The grid fin configurations mainly consist of a baseline model, whose leading edges may be blunt. A typical swept back grid fin configuration having sweptback angle $\Lambda = 30°$, is widely used. Grid fins having sharp leading edges, with leading edge angle $\xi = 20°$ have been tested both experimentally as well as in CFD simulations. *(Figure 2) Table II* summarizes the various geometric configurations of grid fins used for various aerodynamic measurements in both experimentation and CFD simulations. A locally swept back fin is suggested with two new "peak" type and "valley" type interaction as shown in Figure 2. and the intricacies of the geometries discussed in reference [19]. A finite series of five plates approach, is considered to analyze flow through the grid cells in 2D pattern [21]. *Figure 4* shows the plate configuration for 2D simulations.

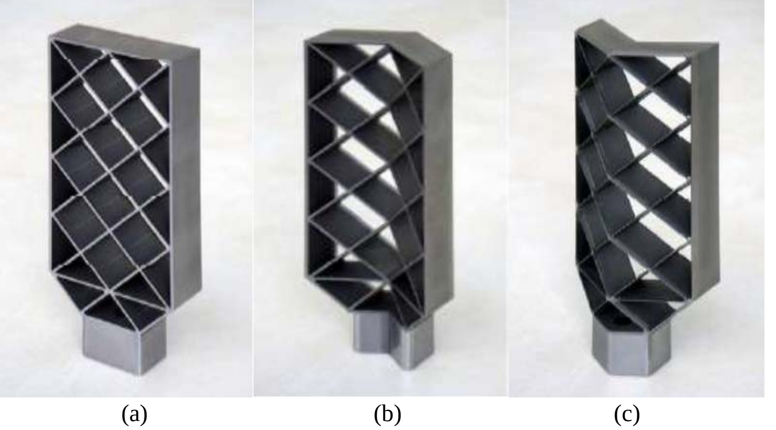

(a) (b) (c)

Figure 2: Images of different grid fin configurations(a) baseline Grid fins, (b) Swept-back Grid fins, (c) Swept-Forward grid fins [14]

Figure 3: A locally sweptback grid fin model configuration [19]

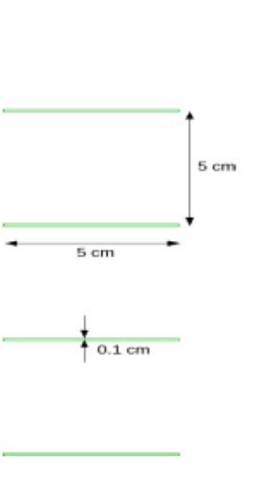

Figure 4: Plate configuration for 2D simulations [21]

Table II: Summary of the various grid fin missile geometries

Reference	Study	Dimensions according to missile diameter D (meters m)/ Calibre	Geometry Features
[3]	CFD & Experimental	D=0.0254m	3D Tangent ogive nose, 13D long cylindrical after body Span s = 0.75D Height h = 0.333D Chord c = 0.118D Case 1: (Baseline) Vane spacing v = 0.1109D Wall Thickness w = 0.007D Case 2: (Thin) Vane spacing v = 0.1139D Wall Thickness w = 0.004D Case 3: (Coarse) Vane spacing v = 0.2288D Wall Thickness w = 0.007D Case 4: (full scale model) Vane spacing v = 0.1985D Wall Thickness w = 0.0015D
[4] **[13]** **[14]** **[15]** **[16]** **[24]** **[29]** **[30]**	CFD & Experimental	D (CFD) = 0.0254m	For CFD for both Baseline and Sweptback Fins 3D Tangent ogive nose, 13D long cylindrical after body, 4 Grid fins in cruciform orientation, Pitch axis 1.5D from rear end Rectangular shaped outer frame Span s = 0.75D Height h = 0.333D Chord c = 0.118D Cell Space = 0.1109D Wall Thickness w = 0.007D Frame swept back $\Lambda = 30^\circ$ Sharp leading edge $\zeta = 20^\circ$ For experimental (Stainless steel body) for both Baseline and Sweptback Fins 07D long cylindrical after body, Pitch axis 1.5D Span s = 0.0857m Height h = 0.0381m Chord = 0.0135m Wall thickness w = 0.0008m
[19]	CFD & Experimental	-	Locally swept back fins Fin thickness = 0.5mm Span s = ∞ Chord c = 10mm Edge sharpness = 10° Local sweep angle φ = 55°& 70°
[20]	CFD & Experimental	D= 0.03m	16 calibers 4 finned canards in line with grid fins 3.7 caliber truncated tangent nose Canard located at 0.96 c caliber from the nose Pitch axis of the grid fins 1.5D from rear end 12.3 caliber long missile body 23 cubic and 12 prismatic webs Span s = 0.74 cal. Chord c = 0.10cal. Thickness t = 0.46cal. Web thickness = 0.003cal.

[21]	CFD	-	2D 5 plates Length 0.05m Thickness 0.001m Spacing 0.05m Rounded leading edge with radius 0.0005m 3D 4 × 3 grids Cell cube dimension 0.05m Thickness t = 0.001m
[28]	CFD	D=0.03m	16 caliber missile body 3D Tangent ogive nose, 13D long cylindrical after body, 4 Grid fins in cruciform orientation, Pitch axis of the fins1.5D from rear end Rectangular shaped outer frame Span s = 0.75D Height h = 0.333D Chord c = 0.118D
[31]	CFD	D=0.127m	10.4calbre missile 3D Tangent ogive nose, 7.4D long cylindrical after body, Pitch axis of the fins 2D from rear end Chord = 0.00975m Web thickness = 0.00020m Fin thickness = 0.00101m Span s = 0.06654m Height h = 0.05334m
[32]	CFD	D=0.0254m	10.4calbre missile 3D Tangent ogive nose, 7.4D long cylindrical after body, Pitch axis of the fins 2D from rear end Chord = 0.00975m Web thickness = 0.00020m

Based on the above-mentioned geometries a basic Grid Fin Missile Geometry can be selected for the CFD analysis. This geometry is shown in Figure *5* consisting of diameter (D=0.0254m) and all the dimensions are in respect of this diameter. The total length of the missile is taken as 16D consisting of tangent ogive nose of length 3D; the fins are attached at a distance of 1.5D ahead of the rear end. The dimensions in *Figure 5* are deliberately in mm to indicate the exact dimensions. Similarly, the recommended intricacies of the Grid Fin Geometry are shown in *Figure 6.*

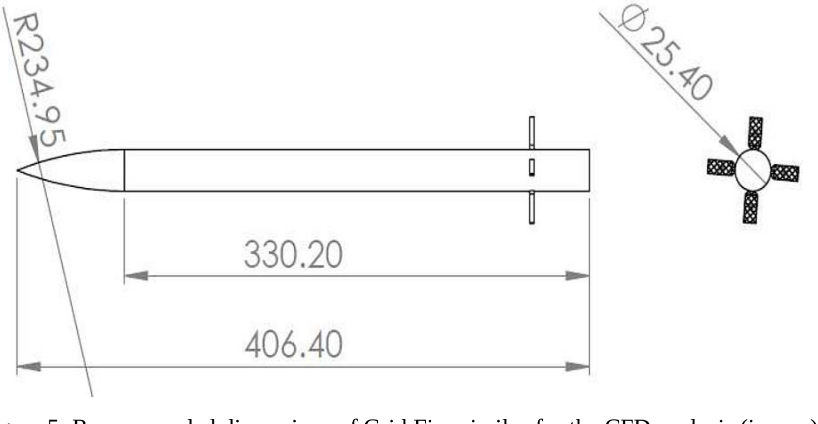

Figure 5: Recommended dimensions of Grid Fin missiles for the CFD analysis (in mm)

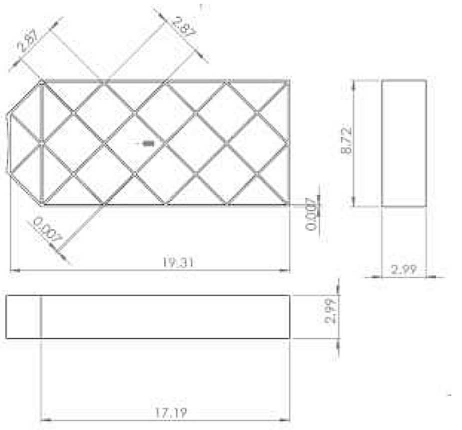

Figure 6: Recommended intricacies of the Grid Fin geometry (in mm)

5. COMPUTATIONAL DOMAIN & MESH VERIFICATION

Meshing of Grid fins, missile and its computational domain is one of the most challenging steps while performing numerical simulations. For the 3D Navier-Stokes equations to be solved, the meshing of the grid fins is a mammoth task, due to the complex geometry. Most of the dense mesh is to be in the grid fin region. To simplify and save the computational time many researchers have used an unstructured mesh inside the Grid cells as well as for the whole computational domain. As the grid fin configuration is symmetrical, the simulations at Zero angle of attack may require only a quarter of geometry for analysis and in some cases even one eighth of geometry has been analyzed, this reducing drastically the computational cost and time. *Table III* summarizes the computational domain and the mesh aspects of the simulations. For the simulations at zero angle of attack, the domain of size as less as 13D or less seems to be sufficient (as implied in many studies), however to have good results for non-zero angle of attack a bigger domain size is suggested to ensure the accuracy of the simulations. The use of both the structured and the unstructured meshes has their own pros and cons, however for higher Reynolds numbers, a structured grid is suggested. For this purpose, a structured hybrid grid is suggested which uses structured grid in most of the grid fin domain. [33] (*Figure 7-10)* An arc-length mesh generation and finite volume has been suggested, [34] *(Figure 11)*. This scheme has been validated with experimental results at Mach 2.5 for various angle of attacks, and shows promising results for future simulations.

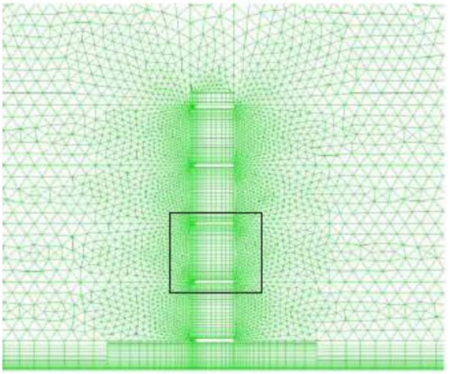

Figure 7: Mesh Details of the Grid fin computational domain [14]

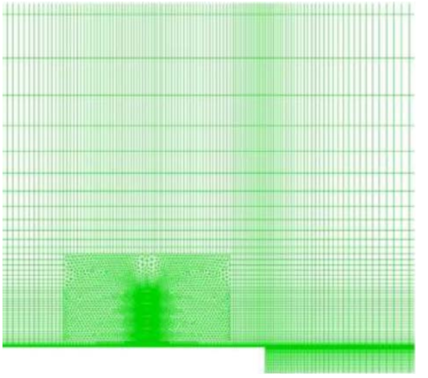

Figure 8: Mesh at the wake region [14]

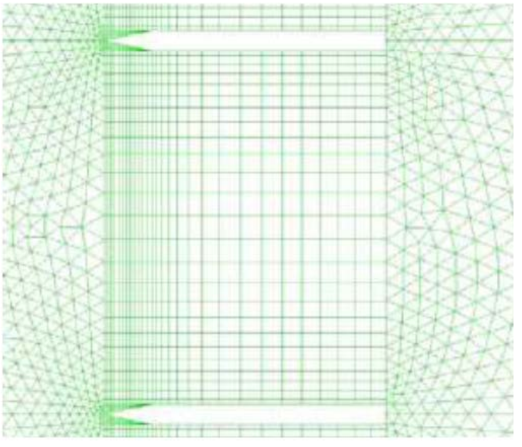

Figure 9: Tetrahedrons with triangle mesh at the edges on the faces of the fins [14]

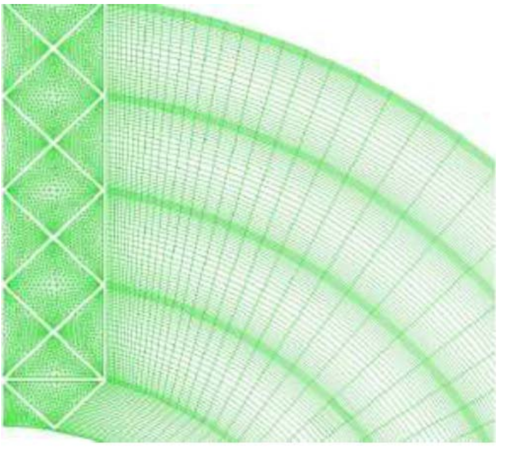

Figure 10: An unstructured mesh is used inside the cell region, with a wedge-shaped mesh in the radial region [14]

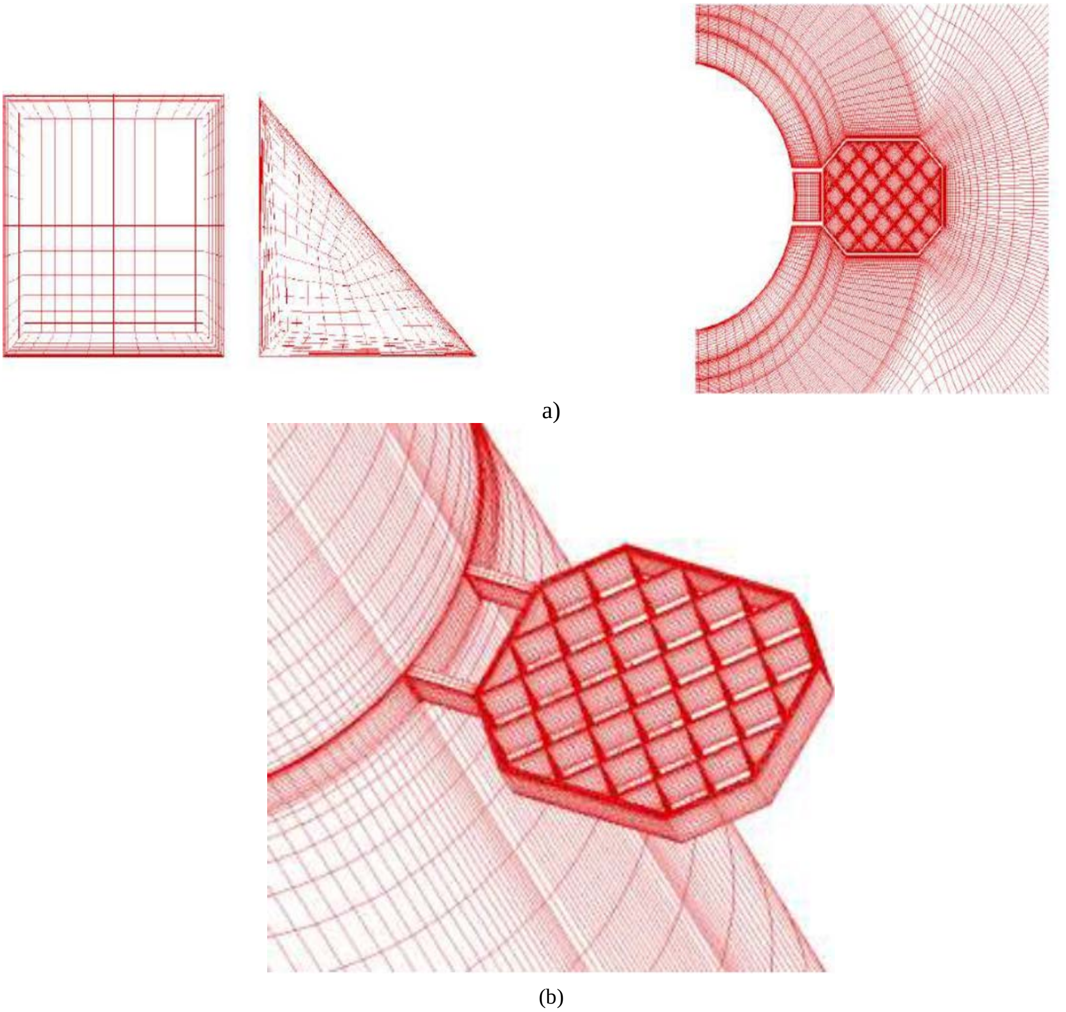

a)

(b)

Figure 11: A hybrid Mesh consisting of majority of structured mesh domain [29]

Table III: Summary of the mesh details

Reference	**Grid Domain / number of cells**	**The boundary Layer Y^+ value and the Growth Factor**	**Mesh/ Domain Features**
[3]	~33 Million cells ~ 6 million nodes	$Y^+ = 1$ Growth Factor/ normal spacing = $3.18841 \times 105D$	Unstructured Volume Grid mesh Mix of tetrahedra/ pentahedral elements
[4]	0.67 million cells for missile with no fins 1.2 million cells for missile with planar fins 3.2 million cells for missile with grid fins	First point of the surface kept at 0.002cal. Mesh stretching was kept below 1.2 $Y+$ = 40-60 along the missile body, 150 along the tangent ogive nose, and between 100-140 on the grid surfaces.	Unstructured mesh Tetrahedral and pyramid transition elements Base flow not simulated hence the mesh stopped at the end of the missile. Computational domain extended 4 calibers from the missile body.
[13]	Upstream & Downstream at 12D of the Missile Body,16D radially from missile cylinder surface 1.2 Million cells	-	Due to model symmetry, only Quarter of Geometry used at Zero angle of attack Symmetry conditions for symmetry surfaces
[14]	Upstream & Downstream at 12D of the Missile Body,16D radially from missile cylinder surface 1.2 Million cells 118 volumes	Y^+ = 0.001D Growth Factor = 1.2 At least 9 points distributed between the boundary layer	Unstructured mesh inside the cells Due to model symmetry, only Quarter of Geometry used at Zero angle of attack Symmetry conditions for symmetry surfaces T type meshing
[15]	Upstream & Downstream at 12D of the Missile Body,16D radially from missile cylinder surface 1.2 Million cells	-	Due to model symmetry, only Quarter of Geometry used at Zero angle of attack Symmetry conditions for symmetry surfaces
[16]	1.2 million cells with 118 entities (volumes) for the 1/8th domain 9.6 million cells for the entire flow domain	-	Due to model symmetry, only one eighth of Geometry used at Zero angle of attack symmetry surfaces
[20]	Mesh extended 50cal. In the liner direction & 66cal in the radial direction 17.3million cells	$Y^+ = 1$ First point of the surface kept at ~ $7.0 \times 10{-}5$ cal. Mesh stretching was kept below 1.25 11 cells in sublayer	Enhanced wall treatment Hexahedral and tetrahedral elements
[21]	For 2D plates ~0.26 million & ~0.34million cells For 3D grid fins ~9million cells	1st layer 2.5×10^{-6m} Growth rate 1.1 Number of layers in the boundary = 34 for 2D mesh For 3D grid $Y^+ = 3.6$ 1st layer 2.5×10^{-6}m Number of layers in the	For 2D grid plate representation Domain: Upstream 0.5c & 150c Downstream 5c & 150c Normal direction 15c and 150c For 3D Domain: Upstream 1c

		boundary = 31	Downstream 5c Normal direction & cross flow 10c Both mesh unstructured
[24]	Upstream & Downstream at 12D of the Missile Body,16D radially from missile cylinder surface 1 Million cells	Y^+ = 0.001D Growth Factor = 1.2 At least 9 points distributed between the boundary layer	only one eighth of Geometry used at Zero angle of attack T type meshing in the transitional sections from fine to coarse meshes.
[28]	Base flow not simulated hence the domain ended with the missile. 3.9 Million cells	First point of the surface between 0.004 and 0.006 caliber Y^+ = between 17-45 for Mach 2 & between 30-60 for Mach 3	Unstructured mesh Mesh stretching below 1.25 Hexahedral and tetrahedral elements ½ plane modelled using symmetry
[29]	Checking for grid independency at 1.20million 1.57million 2.00million 2.48million		"Block off" grid generation method H-O-Type topologies are adopted for the flow field around the fin body shape. Structured grid inside the cells
[30]	~33 Million cells ~ 6 million nodes	Y^+ = 0.37 for vanes and the cells of the grid fins Y^+ = 0.1 to 0.4 for the missile body	Unstructured Volume Grid mesh Mix of tetrahedra/ pentahedral elements
[31]	1.5 million cells	First point of the surface kept at 0.0016D Growth Factor = 1.2 At least 5 rows of boundary layer mesh	T type grid 3D quarter model computational domain
[32]	~ 3 million structured overall ~1.7 million in hybrid out of which ~1.5 million in structured and ~0.2 million in unstructured	-	Multi-block structured grid H-O-Type topologies are adopted for the flow field around the fin body shape.
[33]	-	-	Basic H-O type mesh topologies adopted
[34]	3.2 million cells with 2.5 million cells in the grid fin region	First point of the surface kept at 0.002cal. Mesh stretching was kept below 1.2 Y^+ = 40-60 along the missile body, 150 along the tangent ogive nose, and between 100-140 on the grid surfaces.	Unstructured mesh ½ domain modelled Base flow not simulated

Many researchers have made use of an unstructured mesh, however due to improvement in the meshing tools an approach towards structured mesh can be seen. In case of structured meshes the use of H-O type of mesh topologies is observed. The symmetry of the grid fin is taken as an advantage, by computing only half or one-fourth part of the fin (Applying symmetry boundary condition). The domain taken only till the end of the missile body as the area of interest remains the cells inside the grid fins, which are located ahead of the rear end of the missile.

6. INITIAL BOUNDARY & PHYSICAL CONDITIONS

In most of the cases free stream conditions are applied to the inlet and the outlet of the computational domains. Pressure far-field and non-slip wall condition to the missile body is another common feature of the computational domain. For the 3D RANS model, one equation Spalart-Allmaras turbulent model has been a popular choice for the researchers, though in some cases the two equations $\mathrm{K} - \varepsilon$ and $\kappa - \omega$ turbulence model has also been utilized. A finite volume density based implicit solver is coupled with the turbulence models. A detailed summary of the boundary conditions and the computational domain properties has been provided in *Table IV*.

Table IV: Summary of the Initial Boundary & Physical Conditions

Reference	M_∞	**Pressure (Pa)**	**Temperature (T) (K)**	U_∞ **(m/s)**	**Reynolds Number** Re_D	**Conditions**
[3]	0.744M – 1.190M	-	-	-	4.40 – 7.0 $\times 10^5$	U^2NCLE unstructured flow solver Finite Volume, inviscid solver implicit scheme 2nd order discretization One equation Spalart-Allmaras turbulence model for higher Reynold number.
[4]	2.5M	8325Pa	137K	Free stream conditions	1.26×10^6	Gauss-Seidel, Implicit, 3D compressible RANS solver One equation Spalart-Allmaras turbulence model Freestream boundary conditions
[13]	0.70M - 1.70M	1.17×10^5 -3.25×10^4 Pa	269 – 190K	251 – 496	2.61 - 2.67 $\times 10^6$	Pressure Far-field Non- slip conditions on solid surfaces 3D Navier-Stokes equation Coupled with Spalart-Almaras model One-equation Turbulence model
[14]	0.817M-1.70M	1.11×10^5 - 3.57×10^4 Pa	265-193K	267-473	2.50 – 1.96 $\times 10^6$	3D Navier-Stokes equation Coupled with Spalart-Almaras model Second order, upwind discretization scheme Implicit density based solver Pressure Far-field Symmetry conditions at symmetry surfaces Non- slip conditions on solid surfaces Outlet boundary condition is user defined
[16]	0.817M – 2 M	1atm	295K	-	4.69 – 11.48 $\times 10^5$	3D Navier-Stokes equation Coupled with Spalart-Almaras model Second order, upwind discretization scheme Governing Equations solved using Finite Volume method (FVM) Implicit, density based solver

						Pressure Far-field for outer radial boundary Symmetry conditions for symmetry surfaces Non- slip conditions on solid surfaces
[19]	2M to 6M	-	-	-	-	Finite volume approach to solve Navier-Stokes equations using German developed TAU-code
[20]	0.6M & 0.9M	7.66×10^4Pa & 5.62×10^4Pa	284K & 255K respectively	Free stream conditions	1.01×10^7 & 1.40×10^7	Relizable $K - \varepsilon$ model
[21]	1.1M to 3.0M	-	-	-	0.96×10^6 to 2.6452×10^6	Green-gauss theorem Spalart-Allmaras model Matrix free implicit for convergence acceleration
[24]	0.817M – 2 M	1atm	295K	-	$4.69 – 11.48 \times 10^5$	3D Navier-Stokes equation Coupled with Spalart-Almaras model Second order, upwind discretization scheme Implicit, density based solver Maximum reduction in the residuals by at least 3 orders of magnitude Pressure Far-field for outer radial boundary Symmetry conditions for symmetry surfaces Non- slip conditions on solid surfaces
[28]	2M & 3M	1.268×10^4Pa & 2.77×10^3Pa	166K & 107K	-	3.84×10^5 & 2.34×10^5	Freestream inlet conditions Pressure far-field and outlet conditions Non- slip boundary wall conditions on solid surfaces One equation Spalart-Allmaras turbulence model for higher Reynold number.
[29]	0.7M & 2.5M	-	-	-	5×10^6	One equation Baldwin-Barth model
[30]	0.744M – 2.8M	-	-	-	$7.0 – 26.5 \times 10^6$	CHEM code Navier-Stokes solver MUSCL (flux vector splitting method) scheme for higher order spatial extrapolations $\kappa - \omega$ model with first order discretization
[31]	0.817M – 2M	1atm Free stream conditions	295K Free stream conditions	-	$4.69 – 11.48 \times 10^5$	One equation Spalart-Allmaras model Second order, upwind discretization scheme Implicit, density based solver
[32]	0.7M & 2.5M	Free stream conditions	Free stream conditions	Free stream conditions	5×10^6	MUSCL scheme for higher order spatial extrapolations
[33]	0.7M & 2.5M	Free stream conditions	Free stream conditions	Free stream conditions	5×10^6	Finite volume algorithm solved with LU-SGS
[34]	2.5M	-	-	Free stream conditions	1.26×10^6	Coupled implicit compressible 3D RANS solver using Finite volume method

The physical set up majorly uses freestream conditions, with velocity inlet, pressure far field and outlet conditions. For the 3D RANS equation, the one equation Spalart-Allmaras turbulent model has been extensively used with 2nd order or upwind discretization. Most researches have been done from Mach numbers 0.7M up to 3.0M. An Implicit Density based solver is preferred over the pressure based solver. Due to recent advancements in the computational world, researchers are now also choosing two equations $K-\varepsilon$ & $\kappa-\omega$ turbulent models utilizing third order of discretization for better and accurate results.

7. PRESENTATION OF THE NUMERICAL RESULTS & VERIFICATION & VALIDATION OF THE CFD METHOD

The convergence history of the overall calculation of any aerodynamic coefficient, at a Mach number should be checked to show the oscillations and therefore the stabilization of the simulation to confirm convergence.

The forces as well as the force coefficients are generally shown to be a function of Mach number and in some cases, angle of attack.

The results should be continuously tracked for convergence. Experimental measurements and CFD simulations are widely available for various Mach numbers and for various forces and moments. These are summarized in *Table V* below:

Table V: Results Reference for Verification and Validation

Reference	Measurements	Mach number range	Angle of attack range	Obtained Results/ Aerodynamic coefficients
[13]	Experimental & CFD	0.75M – 1.70M	0° to 12°	Fin Axial Force coefficients, Mach number contours, Normal force coefficients, Pitching moment coefficients
[14]	Experimental & CFD	0.817M – 1.70M	0°	Fin Drag Coefficients, Mach number contours
[15]	Experimental	0.75M – 1.70M	0° to 12°	Fin Drag Coefficients, Overall vehicle axial drag coefficient, Normal force coefficients, Pitching moment coefficients
[16]	CFD	0.905M – 2.0M	0°	Aerodynamic axial force Mach number contours Pressure coefficient contours
[24]	CFD	0.8M-2.0M	0°	Aerodynamic axial force
[17]	CFD	1.5M & 2.0M	0° to 10°	Fin Axial Force coefficients, Mach number contours, Normal force coefficients, Pitching moment coefficients
[3]	Experimental & CFD	0.744M – 1.190M	0°	Fin Axial Force coefficients, Mach number contours, Pitching moment coefficients
[28]	CFD	2M & 3M	0°, 5°, 10°	Axial Force coefficients, Normal force coefficients, Pitching moment coefficients 1200 iterations for convergence
[29]	CFD	0.7M & 2.5M	5°, 10°, 15° &20°	Axial Force coefficients, Normal force coefficients, Bending moments Hinge moments Pressure coefficient contours 5000-6000 iterations for convergence
[30]	Experimental & CFD	0.744M – 2.8M for CFD 0.39M – 1.6M for Experimental	0°	3000 iterations for convergence

[31]CFD	CFD	0.817-2.0M	0°	Maximum residuals reduced to 3rd order of magnitude Axial Force coefficients, Pressure forces Reference area is taken as 1/4th of missile diameter
[19]	CFD & Experimental	2M – 6M	0° to 10°	Pressure coefficients Wave drag coefficients Surface pressure distributions Mach number contours
[32]	CFD	0.7M & 2.5M	5°, 10°, 15° &20°	Normal force coefficients Pressure contours Streamlines distribution
[33]	CFD	0.7M & 2.5M	5°, 10°, 15° &20°	Normal force coefficients Pressure contours Streamlines distribution
[20]	CFD & Experimental	0.6M – 3.0M	0°to 10°	Aerodynamic coefficients Pressure contours
[4]	CFD	2.5M	0°, 10°, 20°	Residuals brought under 10^{-6} 1500 iterations for convergence Axial Force coefficients, Pressure force contours Normal force coefficients
[34]	CFD	2.5M	0°, 10°, 20°	Residuals brought under 10^{-6} Aerodynamic coefficients Pressure contours
[21]	CFD	1.1M- 3.0M	12°to 20°	Lift & drag coefficients Mach number contours

8. CONCLUSIONS

The CFD of grid fins have shown promising results for the analysis of old baseline and new grid fin models. The reduction of drag with minimum effect on the lift of the grid fins has been the most sought out area of investigation.

The normal shocks formed behind the grid structure in the transonic flow are the main cause of choked flow in the grid fin cells. Evidently very less simulations/ experiments have been performed at $\alpha \neq 0$. A wide use of unstructured mesh inside the cells of the grid fins can be seen in the previous literatures. Both Swept-Back and Swept-forward Fins (along with sharp leading edges) can be explored further for the reduction of drag forces in the Grid fins. The experiments of the trans-sonic wind tunnel suggest noteworthy aerodynamic characteristics at Mach numbers 0.90M, 1.09M & 1.30M which can be further explored in CFD while designing a new fin configuration. Swept Back Sharp leading-edge grid fins show considerable drag reduction.

The performance of the Swept-Back sharp leading-edge grid fins can further be explored beyond the trans-sonic regime. The use of unstructured grids has shown consistent results with the experimental counterparts in the transonic regime and the supersonic regime. The choked flow phenomenon can be studied easily from the post process result data of CFD having Mach numbers contour plots. A 2D approach can be useful in understanding the flow characteristics inside the grid fin cells.

Though the majority of the CFD analysis has been performed to calculate static stability derivatives, more of studies using CFD as a tool can be performed to calculate the dynamic stability aerodynamic coefficients in the future.

REFERENCES

[1] A. Misra, *Investigation of Grid and Cascade fins for Missile Flight Stabilization and Control*, Indian Institute of Technology, Kanpur, India, 2009.

[2] M. Khalid, Y. Sun, H. Xu, *Computation of Flows Past Grid Fin Missiles*, in: Missile Aerodyn., RTO MP-5, Sorrento, Italy, pp. 11–14, 1998.

[3] M. C. Hughson, E. L. Blades, G. L. Abate, Transonic Aerodynamic Analysis of Lattice Grid Tail Fin Missiles, *AIAA J*. 1–15, 2006.

[4] J. Despirito, H. L. Edge, P. Weinacht, J. Sahu, Computational Fluid Dynamics Analysis of a Missile with Grid Fins, *AIAA J*. 38, 2001.

[5] M. Miller, W. Washington, An experimental investigation of grid fin drag reduction techniques, *12th Appl. Aerodyn. Conf.*, doi:10.2514/6.1994-1914, 1994.

[6] E. Y. Fournier, *Wind Tunnel Investigation of Grid Fin and Conventional Planar Control Surfaces*, in: 39th Aerosp. Sci. Meet. Exhib. 8-11, AIAA, 2001.

[7] P. Theerthamalai, M. Nagarathinam, Aerodynamic Analysis of Grid-Fin Configurations at Supersonic Speeds, *J. Spacecr. Rockets*., **43**, 750–756, doi:10.2514/1.16741, 2006.

[8] T. Pakkiri, Aerodynamic Characterization of Grid Fins at Subsonic Speeds, *J. Aircr.*, **44**, 694–698, doi:10.2514/1.27653, 2007.

[9] P. Reynier, U. Reisch, J. M. Longo, R. Radespiel, Flow predictions around a missile with lattice wings using the actuator disc concept, *Aerosp. Sci. Technol.*, **8**, 377–388, doi:10.1016/j.ast.2004.03.003, 2004.

[10] P. Reynier, J. M. Longo, E. Schulein, Simulation of Missiles with Grid Fins Using an Actuator Disk, *J. Spacecr. Rockets.*, **43**, 84–91, doi:10.2514/1.7939, 2006.

[11] J. E. Burkhalter, H. M. Frank, Grid fin aerodynamics for missile applications in subsonic flow, *J. Spacecr. Rockets.*, **33**, 38–44, doi:10.2514/3.55704, 1996.

[12] M. Debiasi, *Development of New Grid-Fin Design for Aerodynamic Control*, in: 30th AIAA Appl. Aerodyn. Conf. New Orleans, Louisiana, 25 - 28 June 2012., AIAA, New Orleans, Louisiana, pp. 1–14, 2012.

[13] M. Debiasi, Z. Yan, T. L. Chng, *Swept-Back Grid Fins for Transonic Drag Reduction*, in: 28th AIAA Appl. Aerodyn. Conf., pp. 1–17, doi:10.2514/6.2010-4244, 2010.

[14] M. Debiasi, Measurements of the Forces and Moments Generated by Swept-back Grid Fins, *AIAA Appl. Aerodyn.*, 1–11, 2012.

[15] Y. Zeng, Drag Reduction for Sweptback Grid Fin with Blunt and Sharp Leading Edges, *J. Aircr.*, **49**, 1526–1531, doi:10.2514/1.C031653, 2012.

[16] S. Chen, M. Khalid, H. Xu, F. Lesage, O.- January, F. Lesage, *A Comprehensive CFD Investigation of Grid Fins as Efficient Control Surface Devices*, in: 38th Aerosp. Sci. Meet. Exhib., AIAA, 2000.

[17] G. Abate, G. Winchenbach, W. Hathaway, T. I. B. Committee, *Transonic Aerodynamic and Scaling Issues for Lattice Fin Projectiles Tested in a Ballistics Range*, 19th Int. Symp. Ballist., **1**, 413–420, 2001.

[18] D. Guyot, E. Sch, Novel Locally Swept Lattice Wings for Missile Control at High Speeds, *AIAA J.*, **63**, 2007.

[19] J. Despirito, M. E. Vaughn, W. D. Washington, *Numerical Investigation of Aerodynamics of Canard-Controlled Missile Using Planar and Grid Tail Fins, Part II: Subsonic and Transonic Flow*, 2004.

[20] R. Krishnamurthy, N. Shende, B. Narayanarao, CFD Simulation of grid fin flows, 31st AIAA Appl. Aerodyn. Conf. 24–27, doi:10.2514/6.2013-3023, 2013.

[21] T. W. Ledlow, J. E. Burkhalter, R. J. Hartfield, *Integration of Grid Fins for the Optimal Design of Missile Systems*, in: AIAA Atmos. Flight Mech. Conf., pp. 1–30, doi:10.2514/6.2015-1017, 2015.

[22] W. Washington, P. Booth, M. Miller, *Curvature and Leading Edge Sweep Back Effects on Grid Fin Aerodynamic Characteristics*, in: 11th Appl. Aerodyn. Conf., AIAA, doi:10.2514/6.1993-3480, 1993.

[23] J. Cai, Numerical Study on Choked Flow over Grid-Fin Configurations, *J. Spacecr. Rockets*., **46**, 949–956, doi:10.2514/1.41442, 2009.

[24] E. Y. Fournier, T. I. B. Committee, *Wind Tunnel Investigation of a High L/D Projectile with Grid Fin and Conventional Planar Control Surfaces*, 19th Int. Symp. Ballist., **1**, 511–520, 2001.

[25] J. DeSpirito, M. E. Vaughn, W. D. Washington, Subsonic Flow Cfd Investigation of Canard- Controlled Missile With Planar and Grid Fins, *AIAA J.*, **27**, 1–13, doi:10.2514/6.2003-27, 2003.

[26] A. Despeyroux, J.-P. Hickey, R. Desaulnier, R. Luciano, M. Piotrowski, N. Hamel, Numerical analysis of static and dynamic performances of grid fin-controlled missiles, *J. Spacecr. Rockets.*, **52**, 1236–1252, doi:10.2514/1. A33189, 2015.

[27] J. Despirito, M. E. Vaughn, W. D. Washington, CFD Investigation of Canard-Controlled Missile with Planar and Grid Fins in Supersonic Flow, in: *AIAA J.*, 2002.

[28] J. DeSpirito, J. Sahu, Viscous CFD calculations of grid fin missile aerodynamics in the supersonic flow regime, in: 39th Aerosp. Sci. Meet. Exhib., *AIAA-2001-0257*, doi:10.2514/6.2001-257, 2001.

[29] M. C. Hughson, E. L. Blades, E. A. Luke, *Analysis of Lattice Grid Tailfin Missiles in High-Speed Flow*, 1–15, 2007.

[30] Y. Zeng, J. Cai, M. Debiasi, T. Chng, Numerical Study on Drag Reduction for Grid-Fin Configurations, *New Horizons*, 1–10, doi:10.2514/6.2009-1105, 2009.

[31] H. Lin, J. C. Huang, Navier – Stokes Computations for Body / Cruciform Grid Fin Con guration Introduction, *J. Spacecr. Rockets.*, **40**, 2003.

[32] Y. Q. Deng, M. S. Ma, M. Zheng, N. C. Zhou, Navier-Stokes computation of grid fin missile using hybrid structuredunstructured grids, *Chinese J. Aeronaut.*, **19**, 304–308, doi:10.1016/S1000-9361(11)60332-4, 2006.

[33] M. Ma, Y. Deng, M. Zheng, N. Zhou, Navier-Stokes Computations for a Grid Fin Missile, 23rd AIAA Appl. Aerodyn. Conf. 1–5, doi:10.2514/6.2005-4973, 2005.

[34] J. DeSpirito, H. Edge, P. Weinacht, J. Sahu, S. Dinavahi, *CFD analysis of grid fins for maneuvering missiles*, 38th Aerosp. Sci. Meet. Exhib., doi:10.2514/6.2000-391, 2000.